

# Journal of Materials Chemistry B

Accepted Manuscript



This is an *Accepted Manuscript*, which has been through the RSC Publishing peer review process and has been accepted for publication.

*Accepted Manuscripts* are published online shortly after acceptance, which is prior to technical editing, formatting and proof reading. This free service from RSC Publishing allows authors to make their results available to the community, in citable form, before publication of the edited article. This *Accepted Manuscript* will be replaced by the edited and formatted *Advance Article* as soon as this is available.

To cite this manuscript please use its permanent Digital Object Identifier (DOI®), which is identical for all formats of publication.

More information about *Accepted Manuscripts* can be found in the [Information for Authors](#).

Please note that technical editing may introduce minor changes to the text and/or graphics contained in the manuscript submitted by the author(s) which may alter content, and that the standard [Terms & Conditions](#) and the [ethical guidelines](#) that apply to the journal are still applicable. In no event shall the RSC be held responsible for any errors or omissions in these *Accepted Manuscript* manuscripts or any consequences arising from the use of any information contained in them.

Cite this: DOI: 10.1039/c0xx00000x

www.rsc.org/xxxxxx

ARTICLE TYPE

## Rapid detection of oral cancer using Ag-TiO<sub>2</sub> nanostructured surface-enhanced Raman spectroscopic substrates

Chundayil Madathil Girish,<sup>a</sup> Subramania Iyer,<sup>b</sup> Krishnakumar Thankappan,<sup>b</sup> V. V. Divya Rani,<sup>a</sup> G. Siddaramana Gowd,<sup>a</sup> Deepthy Menon,<sup>a</sup> Shantikumar Nair,<sup>a</sup> Manzoor Koyakutty\*<sup>a</sup>

<sup>5</sup> Received (in XXX, XXX) Xth XXXXXXXXXX 20XX, Accepted Xth XXXXXXXXXX 20XX

DOI: 10.1039/b000000x

Unique vibrational signatures of biochemical changes in tissue samples may enable Raman spectroscopic detection of diseases like cancer. However, the Raman scattering cross-section of tissues is relatively low and hence clinical translation of such methods faces serious challenges. In this study, we report a simple and efficient surface-enhanced Raman scattering (SERS) substrate for the rapid and label-free detection of oral cancer. Raman active silver (Ag) surfaces were created on three distinct titania (TiO<sub>2</sub>) hierarchical nanostructures (needular, bipyramidal and leaf-like) by a process involving hydrothermal reaction followed by sputter deposition of Ag nanoparticles (average size: 30 nm). The resulting SERS substrate efficiencies, measured using crystal violet (CV) as analyte molecule, showed a highest analytical enhancement factor of ~10<sup>6</sup>, detection limit ~1 nM and relative standard deviation of Raman peak maximum ~ 13% for the nano-leafy structure. This substrate was used to analyze tissue sections of 08 oral cancer patients (squamous cell carcinoma of tongue) comprising of total 24 normal and 32 tumor tissue sections and the recorded spectra were analyzed by principal component analysis and discriminant analysis. The tissue spectrums were correctly classified into tumor and normal groups with a diagnostic sensitivity of 100%, specificity of 95.83% and the average processing time per patient is 15-20 min. This indicates the potential translation of SERS method for rapid and accurate detection of cancer.

### Introduction

Raman spectroscopy has been a very effective analytical tool for fingerprinting of molecules based on their vibrational energy levels.<sup>1</sup> Particularly, in biology, the biomolecular fingerprinting can provide plentiful information about the structural conformation of biomolecules as well as the patho-physiological state of cells and tissues based on their biochemical composition.<sup>2-4</sup> Recent studies about the *ex vivo* Raman spectroscopic characterization and classification of tissues from biopsy samples reveals the immense potential of Raman methods for real time analysis of diseased tissues.<sup>5,6</sup> The working principle relies on the detection of unique Raman fingerprints of biological components in various disease conditions. Especially, in cancer, its pathogenesis is always associated with alterations in the expression levels of cellular proteins, lipids, nucleic acids and their conformational states.<sup>7</sup> Diagnostics approaches based on such direct changes in molecular signatures can improve the detection specificity and sensitivity. However, several factors such as low scattering cross-section and tissue auto-fluorescence (while using visible wavelength lasers) resulting in larger spectral integration time and requirement of expensive, background-free optical substrates like quartz, CaF<sub>2</sub> etc (non-usability of glass slides due to interfering low wave number peaks) limited the clinical translation of this technique.

With the emergence of SERS phenomena, limitations due to lower sensitivity of Raman scattering had overcome to greater extent. SERS have been widely utilized for the detection of vibrational signatures of molecules due to its extreme sensitivity and enhancement capability to deliver well-resolved spectral information, when the analyte molecule lies near to a plasmonic metal surfaces (Ag, Au, Cu).<sup>8</sup> Several studies have been reported so far on SERS based approaches to detect protein phosphorylation,<sup>9</sup> DNA hybridization<sup>10</sup>, molecular and live cell imaging<sup>11, 12</sup>, immuno-assay<sup>13</sup> and pathogen detection<sup>14</sup>. Development of SERS platforms for acquisition of enhanced spectral features from cancerous tissue sections can improve the diagnostic reliability. Few studies have reported, demonstrating the potential of enhanced spectral characterization of tumor and normal tissues by incorporating Ag nanoparticles (NP) either on the top of tissue sections or by crushing the tissues and mixing with the NPs.<sup>15,16</sup> For any SERS detection methods, even though the primary requisite is the high enhancement factors, for practical applications and routine analysis, the system should also possess an ease of experimental procedure and handling, inexpensive method for large scale production, stability, and good spectral reproducibility.

Large area nanostructured SERS substrates had overcome the limitations of simple, nanoparticle mediated SERS technique, which involves the lack of reproducibility due to non-uniform distribution of NPs. Various methods such as electron beam

lithography (EBL)<sup>17</sup>, oblique angle deposition (OAD)<sup>18</sup>, nanosphere lithography<sup>19</sup>, template methods etc., were able to generate an array of different plasmonic nanostructured morphologies over large area platforms that were utilized for wide range of applications from characterization of cellular surface to ultrasensitive detection of molecules down to single molecule level.<sup>20,21</sup> Out of these, template methods are often the easiest and inexpensive method that requires nanostructured templates like porous anodic aluminium oxide (AAO) or self-grown nanostructures like nanorods, nanowires, or 3D nanostructures on to which the plasmonic metals are deposited by various techniques.<sup>22-24</sup>

In this study, we have demonstrated a simple and easy fabrication method for the development of Ag-TiO<sub>2</sub> SERS substrates for the rapid detection of oral squamous cell carcinoma. The fabrication of SERS substrate involves a two-step process: hydrothermal synthesis of TiO<sub>2</sub> nanostructures on Ti plate and sputter deposition of Ag NPs on to these nanostructures to generate Raman 'hot spots'. Metal oxides like ZnO, SiO<sub>2</sub>, and TiO<sub>2</sub> are getting wide attention in SERS substrate development because of its easiness to grow controlled array of nanostructures.<sup>25-27</sup> Three different TiO<sub>2</sub> nanostructures named as nano-needular (NN), nano-bipyramidal (NB) and nano-leafy (NL) were synthesized by altering the hydrothermal conditions and their enhancement efficiencies on Ag deposition were studied using standard Raman analyte molecule, CV dye. Even though, a few reports are available on 1D and 2D Ag-TiO<sub>2</sub> based SERS systems<sup>27-29</sup>, this is the first report on the successful fabrication of large area Ag-TiO<sub>2</sub> nanostructured (with three different morphologies) SERS substrates and its utility in cancer detection using clinical samples. As the variations in the overall spectral pattern among tissue types is minimal, in order to understand, evaluate and classify tissue based on the most relevant spectral features from a large collection of spectral dataset, multivariate statistical analysis technique were employed.<sup>5,30,31</sup> Diagnostically significant spectral features from normal and tumor tissues were evaluated and classified using principal component analysis–discriminant analysis (PCA-DA) method.

## Experimental Section

Sodium hydroxide (NaOH), Hexamine (C<sub>6</sub>H<sub>12</sub>N<sub>4</sub>), CV and acetone were purchased from Sigma-Aldrich. Commercially available pure titanium plates (Surgical Grade II, ASTM F-67) were procured from Jayon Surgicals, India. All the polishing silicon carbide grits (Carbimet Paper Discs) were purchased from Buehler Co. Silver (99.99%, 57mm diameter, 0.3mm thickness) target for sputtering were obtained from Ted Pella Inc. Commercial silver SERS substrates were purchased from Yash Nanotech Pvt. Ltd., India.

### SERS substrate fabrication

In the first step, three different nanostructures were synthesized by hydrothermal process as described in our previous work by Divya Rani et al,<sup>32</sup> with some modifications. Briefly, titanium plates (1.5 × 1.5 × 0.2 cm) were polished using silicon carbide grits of various sizes ranging from 600, 1200 and 2400 to make the surface smooth. The polished plates were degreased by ultrasonication in acetone followed by washing with distilled water.

The hydrothermal process was carried out in a teflon lined stainless steel chamber (70 ml volume capacity) by controlling the concentration of solvent, temperature and time duration of the experiment. Three experimental conditions were performed for the synthesis of different nanostructures by immersing the cleaned Ti plates in the teflon chamber containing i) mixture of 20 ml 0.5 M NaOH and 20 ml of 0.5 M hexamine for 5 h at 250 °C, ii) 40 ml of 0.5 M NaOH for 5 h at 250 °C, iii) 40 ml of 0.5 M NaOH for 5 h at 175 °C, which resulted in a formation of NB, NN and NL structures, respectively. For each experimental set up, 04 polished Ti plates were immersed in the teflon chamber without overlapping. After the reaction, the plates were washed with distilled water several times and dried at 60 °C. Second step involves the deposition of Ag NPs onto the nanostructured substrates by magnetron sputtering (Emitech, Peltier-K575X). For all sputtering deposition, the pressure, sputtering current and coating time were maintained at 10<sup>-3</sup> mbar, 40 mA and 100 s, respectively. Distance from target to sample inside the sputter coater was maintained at 40 mm. All the AFM measurements (JEOLJSPM5200) were carried out in tapping mode using super sharp silicon probes (resonance frequency: 330 kHz, spring constant: 42 N/m).

### Sample preparations

For SERS substrate efficiency studies, CV solutions with serial concentrations ranging from 100 μM to 1 nM were prepared in distilled water and 10 μl of the solution was drop casted on the substrates, followed by air drying. Tissue samples were acquired during surgical excision of suspicious lesions from the oral cavity of patients with their proper consent and by the full approval from Institute Ethical Committee (IEC) at Amrita Institute of Medical Sciences & Research Centre, Cochin. Eight patients were included in the study, diagnosed with oral squamous cell carcinoma of tongue. Excised tissues were washed in cold PBS (to remove blood content), snap frozen immediately after excision and transferred to -80 °C until use. Alternate cryosections were obtained for Raman studies (7-9 μm thickness) in freshly prepared Ag-NL substrates as well as for hematoxylin & eosin staining (H&E staining; 4 μm thick) in poly lysine coated glass slides.

### Characterizations

The morphology and composition of the nanostructures were characterized using SEM (JEOLJSM 6420), FESEM (Hitachi SU660), TEM (JEOL 3010) and energy dispersive analysis (EDS) respectively. X-Ray powder diffraction analysis was carried out by Panalytical X'pert Pro-diffractometer which revealed the crystalline phase of the nanostructured materials. SERS measurements were carried out in WITec alpha 300RA confocal microscope system comprising of a UHTS 300 spectrometer (600 lines/mm grating) coupled with a peltier cooled CCD detector. A laser wavelength of 488 nm from a DPSS source was used to excite the sample, guided via optical fiber of diameter 100 μm, which was focused on to the sample by a 50X objective lens (NA-0.8). For all the CV experiments, the laser power was maintained approximately at 50 μW with an integration time and number of acquisitions as 0.5 s and 10, respectively. All the tissue spectral measurements were carried out at a laser power of nearly 100 μW with an integration time

and number of accumulations as 3 s and 10, respectively. The instrument was calibrated using a standard silicon sample peak at  $520\text{ cm}^{-1}$ .

### 5 Raman spectral analysis

Spectral data acquired from tissue sections in the range of  $500\text{--}1800\text{ cm}^{-1}$  were selected for our studies and subjected to auto-polynomial background correction and normalization, cosmic ray removal and 3<sup>rd</sup> order averaging using WITec Project Plus software. Further the spectral data were analyzed and classified by multivariate analysis (PCA-DA) method using XLSTAT Pro (Addinsoft). PCA is used to reduce the complexity of data and to identify most relevant spectral features related to normal and tumor tissues from large number of spectral dataset. By utilizing PCA, it reduces the dimension of the large spectral dataset in to a few principal components (PC) that represents the total dataset without losing any meaningful information. PCs are formed in such a way that the first principal component (PC1) shows the spectral features that shows the maximum variance in the total dataset where as the succeeding components shows the spectral features in the order of decreasing variance. Each spectral loadings of a particular PC is related to the individual spectrum by a PC score value. Diagnostically significant PCs were identified using Student's t-test ( $p < 0.05$ ) and their corresponding PC score values were considered for the classification of normal and tumor spectra using DA. DA use statistical functions to generate discriminant scores based on the spectral attributes that defines each group and predicts each observation in to their corresponding groups. The entire spectral acquisition from tissues and its classification were carried out within time duration of 2 h.

## Results and Discussion

### SERS substrate characterization

The SEM, XRD and EDS analysis reveal the morphology and composition of three different nanostructures as shown in Fig. 1. Fig. 1a shows the smooth surface of polished Ti plate in which different nanostructures are grown (Inset shows the photographic image of unpolished Ti plate). NB structures (Fig. 1b) have an effective width around  $400\text{--}500\text{ nm}$  at the center which tapers towards two ends with an end diameter  $\sim 100\text{ nm}$ . For NN structures (Fig. 2c), the diameter was around  $50\text{--}120\text{ nm}$  and length ranging from  $1\text{--}3\text{ }\mu\text{m}$ . In case of NL structures (Fig. 2d), nanostructures appear as un-oriented leaflets with inter-leaf spacing of  $20\text{--}150\text{ nm}$ . Fig. 2e shows XRD patterns of nanostructures indicating major rutile phase (JCPDS-01-076-0323) with traces of anatase content (JCPDS-01-071-1169). In case of NL, the peak at  $2\theta$  value  $25^\circ$  is completely absent compared to NN and NB structures. In NN structure, the presence of an impurity peak of sodium titanate (S) is detected at  $28^\circ$  whereas all other peaks were not seen. Fig. 2f shows the typical EDS spectrum of  $\text{TiO}_2$  nanostructure that mainly constitutes Ti, O and traces of Na. The formation of different nanostructures on polished Ti plates can be explained on the basis of dissolution and re-precipitation mechanisms.<sup>32</sup> Ti dissolute into the solution as  $\text{Ti}(\text{OH})^{3+}$  ions and re-precipitates back onto the plates as  $\text{TiO}_2$ ,

in the presence of aqueous alkali at hydrothermal conditions. The morphology of different structures could be tuned by changing various reaction conditions such as temperature and concentration of NaOH and hexamine. At  $175^\circ\text{C}$ ,  $\text{pH} \sim 12$ , a unique leaf-like structure was formed. By increasing the temperature to  $250^\circ\text{C}$ , the precipitation rate increases resulting in a needular morphology. At the same temperature, when hexamine was used as a chelating agent that restricts the reaction kinetics and availability of metal ions from the solution, a bipyramidal nanostructure was obtained.<sup>32</sup>

For making the above nanostructures Raman active, Ag NPs were sputter deposited on these nanostructures under optimized conditions and the SERS enhancements as well as deposited nanoparticle size were characterized. Four different sputtering durations of 25, 50, 75 and 100 s at constant sputtering current 40 mA were studied. Raman measurements were carried out on Ag sputtered NB substrates coated at 40 mA for above mentioned sputtering durations. It was observed that sputtering for 100 s provided maximum SERS intensity and uniform spectrum from various spots (Fig. S1, ESI<sup>†</sup>). In order to understand the pattern of nanoparticle formation, atomically flat mica sheets were also placed along with NB substrates during sputtering. Fig. 2a-c shows the AFM topographic images of Ag sputtered mica sheet coated at 40 mA for duration of 25, 50 and 100 s. These images show the increasing trend in formation of bigger nanoparticles ( $200\text{--}500\text{ nm}$ ) when the sputtering time increased from 25 to 100 s, which may be explained due to the coalescence effect.<sup>33</sup> Fig. 2d-f shows the AFM topographic images of NB substrates before (Fig. 2d) and after (Fig. 2e, f) sputtering with Ag for 100 s. AFM topographic image from Ag-NB reveals that the average size of deposited NPs is around  $30\text{ nm}$  (Fig.2f). Since the nanostructures increase the surface area for Ag deposition enormously, the coalescence observed at higher sputtering durations from mica sheet is very much reduced from the nanostructured substrate.<sup>34</sup> In similar manner, all other nanostructures were coated with Ag NPs of same size and sputtering conditions. Fig. 3 shows the FESEM image (Fig. 3a-d), TEM image (Fig. 3e) and XRD (Fig. 3f) pattern of the Ag sputtered nanostructures. Although, we could not get a high resolution image for deposited NPs on NL structure, FESEM images shows that after sputter deposition, the effective wall thickness of NL was increased from  $20 \pm 3\text{ nm}$  to  $44 \pm 4\text{ nm}$  (Fig. 3b, d). TEM analysis of Ag-NN structures (scratched from Ti plates and dispersed in acetone) reveals that the deposited Ag nanoparticles have an average size nearly  $30\text{ nm}$  (Fig. 3f). The presence of Ag was shown in the XRD spectra of NL structures at  $2\theta$  value  $44.2^\circ$  and  $64.42^\circ$ , while the Ag peak at  $38.1^\circ$  overlaps with the Ti peak (Fig. 3f). In Ag-NL, the elemental composition (atomic percentage) constituted by Ti, O, Ag were  $29.71$ ,  $60.04$  and  $3.30$ , respectively (Fig. S2, ESI<sup>†</sup>).

We have used the above synthesized substrates for SERS investigations. To quantify the enhancement effect, we have calculated the enhancement factor of substrates by measuring the ratio between Raman scattering intensities of CV peak with and without SERS. CV shows major characteristic peaks at  $914\text{ cm}^{-1}$  (ring skeletal vibration of radical orientation),  $1175\text{ cm}^{-1}$  (ring C-H bend, in-plane vibration)  $1371\text{ cm}^{-1}$  (N-phenyl stretching),  $1588\text{ cm}^{-1}$  (ring C-C stretching),  $1619\text{ cm}^{-1}$  (ring C-C stretching).<sup>35</sup> Even though there are many approaches to

determine the enhancement factor,<sup>36</sup> we have calculated the analytical enhancement factor which determines the enhancement for a given analytical volume of sample with and without SERS, based on the equation<sup>37,38</sup>

$$E F = (I_{\text{SERS}}/I_{\text{NR}}) \times (C_{\text{NR}}/C_{\text{SERS}})$$

where  $I_{\text{SERS}}$  and  $I_{\text{NR}}$  corresponds to Raman intensities of 1588  $\text{cm}^{-1}$  peak with SERS effect from Ag-TiO<sub>2</sub> substrates and normal scattering recorded from CaF<sub>2</sub> slides while  $C_{\text{SERS}}$  and  $C_{\text{NR}}$  represents the corresponding concentration of CV in these substrates, respectively (reference concentrations taken as 10 mM). The averaged analytical enhancement factor calculated for Ag-TiO<sub>2</sub> substrates were estimated nearly  $1 \times 10^6$  for NL and  $9 \times 10^5$  for NB and NN structures.

To know the enhancement effect generated by the nanostructures, CV spectrum was also measured from polished Ti plates sputtered with Ag at same conditions as well as from a commercial silver SERS substrate. Fig. 4A shows averaged SERS spectra of CV (10  $\mu\text{M}$ ) obtained from three different TiO<sub>2</sub> nanostructures (NB, NN, NL) sputtered with Ag. Out of the three structures, NL showed highest enhancement whereas NN and NB structures showed almost similar enhancement. The spectral intensity at 1588  $\text{cm}^{-1}$  from commercial Ag-SERS substrate, NN, NB and NL substrates were nearly 10, 90, 94, 130 times higher, respectively, compared to Ag coated polished Ti plates. Generally, enhancement effects from nanostructured plasmonic surfaces are mainly contributed by favorable surface geometries that facilitates localized plasmonic resonance between the incident photons and plasmons.<sup>8,39</sup> Typical geometric features that promotes high local field enhancement includes surface roughness, sharp edges, tips and junctions or gaps between plasmonic NPs that serves as 'hot spots' for field enhancement compared to individual NPs.<sup>40,41</sup> In case of Ag NP coated nanostructures (TiO<sub>2</sub>), these hot spots may form either between two nearby nanoparticles on the same nanostructure (intra-structure contribution) and/or the nanoparticles on adjacent nanostructures (inter-structure contribution). The intra-structure contribution may vary with the NPs concentration while inter-structure contribution will depend on the morphology (needular, bipyramidal, leaf-like, etc), inter-structure distance (structure density per unit area) and nanoparticle size.<sup>39</sup> Considering these aspects, we have examined the possible contributions leading to SERS enhancement in our NN, NB and NL structures.

In Fig. 5, left panel shows SEM images of NN, NB, NL structures within an area of 1  $\mu\text{m}^2$  and right panel shows the schematic representation of possible hot spot formation in these structures. For Ag-NN, the sites of enhancement can be between Ag NPs on the surface of needleless (intra-structure, denoted as 'a' in Fig. 5 schematic) and/or between needles (inter-structures, denoted as 'b' in Fig. 5 schematic). However, recently, Deng et al., reported that the inter-structure enhancement is prominent only if the size of the NPs are relatively large ( $\geq 150\text{nm}$ ).<sup>37</sup> In case of smaller size particles ( $\sim 10\text{nm}$ ), intra-structure contribution is prominent. In our case of NN, the average size of Ag nanoparticle was  $\sim 30\text{nm}$  and the averaged inter-structure distance between needles were relatively high ( $\sim 350\text{nm}$ ). Hence, probably, the possibility of inter-needle enhancement is relatively low. In case of NB, the enhancement can be contributed by NPs on the faces,

edges, tips and between the bipyramidals. However, from the SEM images, it is clear that 2 to 5 pyramidal structures are seen within 1  $\mu\text{m}^2$  area. Whereas in NL structure, large number of closely packed leaf-like nanostructure with an average inter-structure spacing of 20-150 nm can be seen. In addition, leaf-like morphology provides more adjacent parallel surfaces than unaligned needles or bipyramidals. The Ag NPs on each of these closely packed adjacent leaf-like surfaces can contribute to the formation of more inter-structure hot spots than any other structures. This may explain the observed higher SERS enhancement in NL compared to NB and NN. However, detailed simulation studies may be needed to quantify the exact field enhancement prevailing in these distinct nanostructures.

Further, to study the limit of detection in NL structure, we measured CV spectrum for a wide range of molar concentrations ranging from 100  $\mu\text{M}$  to 1 nM. Fig. 6A shows the SERS spectrum of different CV concentrations from Ag-NL substrates. From the plot, it is clear that 100  $\mu\text{M}$  shows the maximum intensity and all five CV characteristic peaks were visible up to 10 nM. Even though the noise levels were high in 1 nM CV spectrum, the main characteristic peaks of CV at 1175, 1371, 1588 and 1619  $\text{cm}^{-1}$  were clearly visible as shown in the inset. To assess the reproducibility, relative standard deviations (RSD) of the major peak intensities were measured. From recent reported studies, it is understood that the RSD value for an efficient SERS substrates should be within 20%.<sup>26, 42</sup> For calculating the RSD value, we have measured the SERS signal intensity of four major characteristic peaks of CV (10  $\mu\text{M}$ ) from the Ag-NL substrates, obtained from 10 randomly selected points (Fig. 6B). The RSD value of the peaks at 1175, 1371, 1588 and 1619  $\text{cm}^{-1}$  were measured as 10%, 16%, 12% and 10%, respectively (average: 13%). From Fig. 6B, it is clear that the spectrum were highly uniform with insignificant variations in the intensities, probably due to some non-uniformity in the Ag deposition.

#### Oral cancer detection using SERS substrates

As the Ag-NL substrate showed highest SERS enhancement, we used this substrate for all further studies on the detection and classification of tumor versus normal tissues from oral cancer patients. For SERS phenomena to happen, one of the main criteria is the close proximity of tissue with SERS substrate. In this case, it is achieved by the quick adsorption of cryosections on to Ag-NL substrate due to prevailing temperature difference between the substrate (normal room temperature) and tissue cryosections (nearly  $-20^\circ\text{C}$ ). Spectrums were acquired from the tissue-substrate interface which was identified by the sudden increase in spectral intensity and reduction of fluorescence, upon depth profiling. Fig. 7 shows the averaged SERS spectra of tumor and normal tissues obtained from Ag-NL substrates as well as H&E stained images of tissue sections. H&E stained images confirmed the malignant and normal pathology of tissue sections. Characteristic features of tumor showed high cellular and nuclear pleomorphism, more mitotic cells and highly invaded connective tissue regions whereas normal sections showed longitudinally and transversely arranged connective tissue with few numbers of cells. Similar to the previous studies reported, the major changes associated with spectral signatures recorded relates to characteristic peak assignments of proteins, amino acids, nucleotides and lipids.<sup>31,43-47</sup> The major intense peaks common in

both normal and tumor spectra are around 728 (C-N stretching), 870 (C-C stretching), 946 (C-C stretching), 1012 (symmetric ring breathing, phenylalanine), 1100 (C-C/C-N stretching), 1260 (amide III/C-H deformation), 1460 (CH<sub>2</sub> bending), 1672 (amide I) and 1750 cm<sup>-1</sup> (C=O stretching). In addition, tumor spectra showed more intense peak positions contributed especially by aromatic amino acids (phenyl alanine, tryptophan, and tyrosine) and nucleotides at 645, 680, 794, 825, 1189, 1326, 1585, and 1618 cm<sup>-1</sup>. Normal tissue spectra was characterized by intense peak position assigned by the collagen from connective tissue at 870 and 950cm<sup>-1</sup>, less intense peak of phenyl alanine and protein/nucleotide at 1012 and 1326 cm<sup>-1</sup>, respectively. These unique tissue specific spectral characteristics can be used to classify normal and tumor tissue types which in turn were identified using PCA, from a large spectral dataset.

Diagnostically significant spectral features related to tumor and normal tissue types were represented by the first five PCs (estimated by Student's t-test,  $p < 0.05$ ; Fig.S3, ESI<sup>†</sup>). Fig. 8A shows the contribution of spectral peak positions in the first five significant PCs that represents all the major peak assignments related to proteins, lipids, nucleotides and aromatic amino acids, discussed above. Further, these PCs were used for classification of tumor and normal tissues using DA. Fig. 8B shows the discriminant analysis biplot showing the classification of each spectrum (normal as circle, tumor as square) to the respective tumor or normal groups based on the linear discriminant scores. Out of 32 tumor spectra, all were classified correctly into tumor group, whereas one out of 24 normal spectra was wrongly classified in to tumor group. This refers to a sensitivity of 100%, which defines test's ability to correctly identify positive results (tumor, 32/32) and specificity of 95.83%, which defines the test's ability to correctly identify negative results (normal, 23/24) (Table T1, ESI<sup>†</sup>). The enhanced spectral signatures from tissue sections acquired using Ag-TiO<sub>2</sub> SERS substrate provided an overall accuracy (55/56) of about 98.21% towards detection of normal and tumor tissues. This is achieved because of the presence of enhanced spectral discriminating features related to tumor and normal tissue composition, carried by each individual spectrum. This method allows for an improved accuracy rate on tumor and its subtype detection in the context of prevailing studies reported on Raman spectroscopy based cancer detection.<sup>5,41</sup> As the entire procedure takes only few minutes for spectral acquisition and classification, our study projects the potential of SERS mediated faster diagnosis of cancer.

## Conclusions

In summary, we have demonstrated the potential application of Ag-TiO<sub>2</sub> SERS substrate for the rapid detection of oral cancer with 100% sensitivity. Three unique TiO<sub>2</sub> nanostructures (needular, bipyramidal and leaf-like) were grown by hydrothermal method and a uniform coating of Ag nanoparticles was made by magnetron sputtering. The substrate efficiencies were monitored by measuring the peak intensities of CV spectrum. Leaf-like Ag-TiO<sub>2</sub> nanostructures showed highest analytical enhancement factor of ~10<sup>6</sup>, minimum detectable concentration ~ 1 nM and RSD of Raman peak maximum ~ 13%. The enhanced spectral signatures of tissue sections from 08 patients (consisting of 24 normal and 32 tumor spectra) were

obtained using Ag-NL substrates and classified with the help of PCA-DA method to successfully detect cancer tissue with a specificity and sensitivity of 95.83% and 100%, respectively. Thus, we show the potential of Ag-TiO<sub>2</sub> SERS substrate for the diagnosis oral squamous cell carcinoma by Raman histopathology. These substrates may also be used for other tumor types and further experiments are in progress for the staging of tumor grades.

## Acknowledgement

We thank Department of Biotechnology, Govt. of India for the financial support under the project "Oncogene sensing and Finger-printing from saliva using Nanotechnology enabled Raman Spectroscopy" (Project No: BT/PR11796/MED/32/102/2009). One of the authors Girish C M is thankful to Council of Scientific and Industrial Research, Govt. of India, for providing the Senior Research Fellowship (Ref. No:9/963(0015)2K11-EMR1). We thank School of Nanosciences, NIT Calicut and DST Unit of Nanosciences, IIT Chennai for helping to carry out the FESEM and TEM measurements, respectively. We also thank Mr. Sajin P Ravi for his support on electron microscopy analysis.

## Notes and references

- <sup>80</sup> <sup>a</sup> Amrita Centre for Nanosciences & Molecular Medicine, Amrita Vishwa Vidyapeetham University, Cochin, India- 682041  
Fax: +91 484 2802030; Tel: +91 484 4008750  
E-mail: [manzoork@aims.amrita.edu](mailto:manzoork@aims.amrita.edu)
- <sup>85</sup> <sup>b</sup> Department of Head and Neck Surgery, Amrita Institute of Medical Sciences, Cochin, India- 682041
- <sup>†</sup> Electronic Supplementary Information (ESI) available: includes Raman spectra comparison, EDAX spectra and details of PCA-DA results. See DOI: 10.1039/b000000x/
- 1 J. De Gelder, K. De Gussem, P. Vandenabeele and L. Moens, *J. Raman Spectrosc.*, 2007, 38, 1133
  - 2 C. J. Frank, R. L. McCreery and D. C. B. Redd, *Anal. Chem.*, 1995, 67, 777
  - 3 A. Downes, R. Mouras, P. Bagnaninchi and A. Elfick, *J. Raman Spectrosc.*, 2011, 42, 1864
  - 4 N. C. Maiti, M. M. Apetri, M. G. Zagorski, P. R. Carey and V. E. Anderson, *J. Am. Chem. Soc.*, 2004, 126, 2399
  - 5 N. Stone, C. Kendall, N. Sheperd, P. Crow and H. Barr, *J. Raman Spectrosc.*, 2002, 33, 564
  - 6 N. D. Magee, J. S. Villaumie, E. T. Marple, M. Ennis, J. S. Elborn and J. J. McGarvey, *J. Phys. Chem. B*, 2009, 113, 8137
  - 7 J. R. Mourant, K. W. Short, S. Carpenter, N. Kunapareddy, L. Coburn, T. M. Powers and J. M. Freyer, *J. Biomed. Opt.*, 2005, 10, 031106
  - 8 P. L. Stiles, J. A. Dieringer, N. C. Shah and R. P. Van Duyne, *Annu. Rev. Anal. Chem.*, 2008, 1, 601
  - 9 S. Siddhanta, D. Karthigeyan, P. P. Kundu, T. K. Kundu and C. Narayana, *RSC Advances*, 2013, 3, 4221
  - 10 R. P. Johnson, J. A. Richardson, T. Brown and P. N. Barlett, *J. Am. Chem. Soc.*, 2012, 134, 14099
  - 11 C. L. Zavaleta, E. Garai, J. T. C. Liu, S. Sensam, M. J. Mandella, D. V. Sompel, S. Friedland, J. V. Dam, C. H. Contag and S. S. Gambhir, *Proc. Natl. Acad. Sci. U S A*, 2013, 110, E2288
  - 12 G. Zhang, G. Qu, Y. Chen, A. Shen, W. Xie, X. Zhou and J. Hu, *J. Mater. Chem. B*, 2013, 1, 4364
  - 13 Y. Pei, Z. Wang, S. Zhong and Y. Cui, *J. Mater. Chem. B*, 2013, 1, 3992

- 14 X. Zhang, M. A. Young, O. Lyandres and R. P. Van Duyne, *J. Am. Chem. Soc.*, 2005, 127, 4484
- 15 S. Feng, J. Lin, Z. Huang, G. Chen, W. Chen, Y. Wang, R. Chen and H. Zeng, *Appl. Phys. Lett.*, 2013, 102, 043702
- 16 O. Aydin, M. Altas, M. Kahraman, O. F. Bayarak and M. Culha, *Appl. Spectrosc.*, 2009, 63, 1095
- 17 A. Nahla, A. Hatab, J. M. Oran and M. J. Sepaniak, *ACS Nano*, 2008, 2, 377
- 18 S. B. Chaney, S. Shanmukh, R. A. Dluhy and Y. P. Zhao, *Appl. Phys. Lett.*, 2005, 87, 031908
- 19 A. V. Whitney, J. W. Elam, P. C. Stair and R. P. Van Duyne, *J. Phys. Chem. C.*, 2007, 111, 16827
- 20 T. T. Liu, Y. H. Lin, C. S. Hung, T. J. Liu, Y. Chen, Y. C. Huang, T. H. Tsai, H. H. Wang, D. W. Wang, J. K. Wang, Y. L. Wang and C. H. Lin, *PLoS ONE*, 2009, 4, e5470
- 21 H. Liu, L. Zhang, X. Lang, Y. Yamaguchi, H. Iwasaki, Y. Inouye, Q. Xue and M. Chen, *Sci. Rep.*, 2011, 1, 112
- 22 G. Sinha, L. E. Depero and I. Alessandri, *ACS Appl. Mater. Interfaces*, 2011, 3, 2557
- 23 E. Galopin, J. Barbillat, Y. Coffinier, S. Szunerits, G. Patriarche and R. Boukherroub, *ACS Appl. Mater. Interfaces*, 2009, 1, 1396
- 24 C. Cheng, B. Yan, S. M. Wong, X. Li, W. Zhou, T. Yu, Z. Shen, H. Yu and H. J. Fan, *ACS Appl. Mater. Interfaces*, 2010, 2, 1824
- 25 H. Y. Wu and B. T. Cunningham, *Appl. Phys. Lett.*, 2011, 98, 153103
- 26 F. Xu, Y. Zhang, Y. Sun, Y. Shi, Z. Wen and Z. Li, *J. Phys. Chem. C*, 2011, 115, 9977
- 27 X. Li, G. Chen, L. Yang, Z. Jin and J. Liu, *Adv. Funct. Mater.*, 2010, 20, 2815
- 28 L. Yang, X. Jiang, W. Ruan, J. Yang, B. Zhao, W. Xu and J. R. Lombardi, *J. Phys. Chem. C*, 2009, 113, 16226
- 29 A. Roguska, A. Kudelski, M. Pisarek, M. Opara and M. J. Czachor, *Vib. Spectrosc.*, 2011, 55, 38
- 30 S. K. Teh, W. Zheng, K. Y. Ho, M. Teh, K. G. Yeoh and Z. Huang, *Br. J. Cancer*, 2008, 98, 457
- 31 S. P. Singh, A. Sahu, A. Deshmukh, P. Chaturvedi and C. Murali Krishna, *Analyst*, 2013, 138, 4175
- 32 V. V. Divya Rani, K. Manzoor, D. Menon, N. Selvamurugan and S. V. Nair, *Nanotechnology*, 2009, 20, 195101
- 33 A. Merlen, V. Gadenne, J. Romann, V. Chevallier, L. Patrone and J. C. Valmalette, *Nanotechnology*, 2009, 20, 215705
- 34 N. Nuntawong, M. Horprathum, P. Eiamchai, K. Wong-ek, V. Pathanasattakul and P. Chindaudom, *Vacuum*, 2010, 84, 1415
- 35 M. Sackmann, S. Bom, T. Balster and A. Materny, *J. Raman Spectrosc.*, 2007, 38, 277
- 36 E. C. Le Ru, E. Blackie, M. Meyer and P. G. Etchegoin, *J. Phys. Chem. C*, 2007, 111, 13794
- 37 S. Deng, H. M. Fan, X. Zhang, K. P. Loh, C. -L. Cheng, C. H. Sow and Y. L. Foo, *Nanotechnology*, 2009, 20, 175705
- 38 W. H. Hsiao, H. Y. Chen, Y. C. Yang, Y. L. Chen, C. Y. Lee and H. T. Chiu, *ACS Appl. Mater. Interfaces*, 2011, 3, 3280
- 39 R. J. C. Brown, J. Wang and M. J. T. Milton, *J. Nanomater.*, 2007, 2007, 12086
- 40 T. Y. Jeon, S. G. Park, S. Y. Lee, H. C. Jeon and S. M. Yang, *ACS Appl. Mater. Interfaces*, 2013, 5, 243
- 41 H. Ko, S. Singamaneni and V. V. Tsukruk, *Small*, 2008, 4, 1576
- 42 M. Fan and A. G. Brolo, *Phys. Chem. Chem. Phys.*, 2009, 11, 7381
- 43 Y. Li, J. Pan, G. Chen, C. Li, S. Lin, Y. Shao, S. Feng, Z. Huang, S. Xie, H. Zeng and R. Chen, *J. Biomed. Opt.*, 2013, 18, 27003
- 44 S. K. Teh, W. Zheng, D. P. Lau and Z. Huang, *Analyst*, 2009, 134, 1232
- 45 M. S. Bergholt, K. Lin, W. Zheng, D. P. C. Lau and Z. Huang, *J. Biomed. Opt.*, 2012, 17, 077002
- 46 L. E. Kamekoto, A. K. Misra, S. K. Sharma, M. T. Goodman, H. Luk, A. C. Dykes and T. Acosta, *Appl. Spectrosc.*, 2010, 64, 255
- 47 K. Venkatakrishna, J. Kurien, K. M. Pai, M. Valiathan, N. N. Kumar, C. Murali Krishna, G. Ullas and V. B. Kartha, *Current Sci.*, 2001, 80, 665

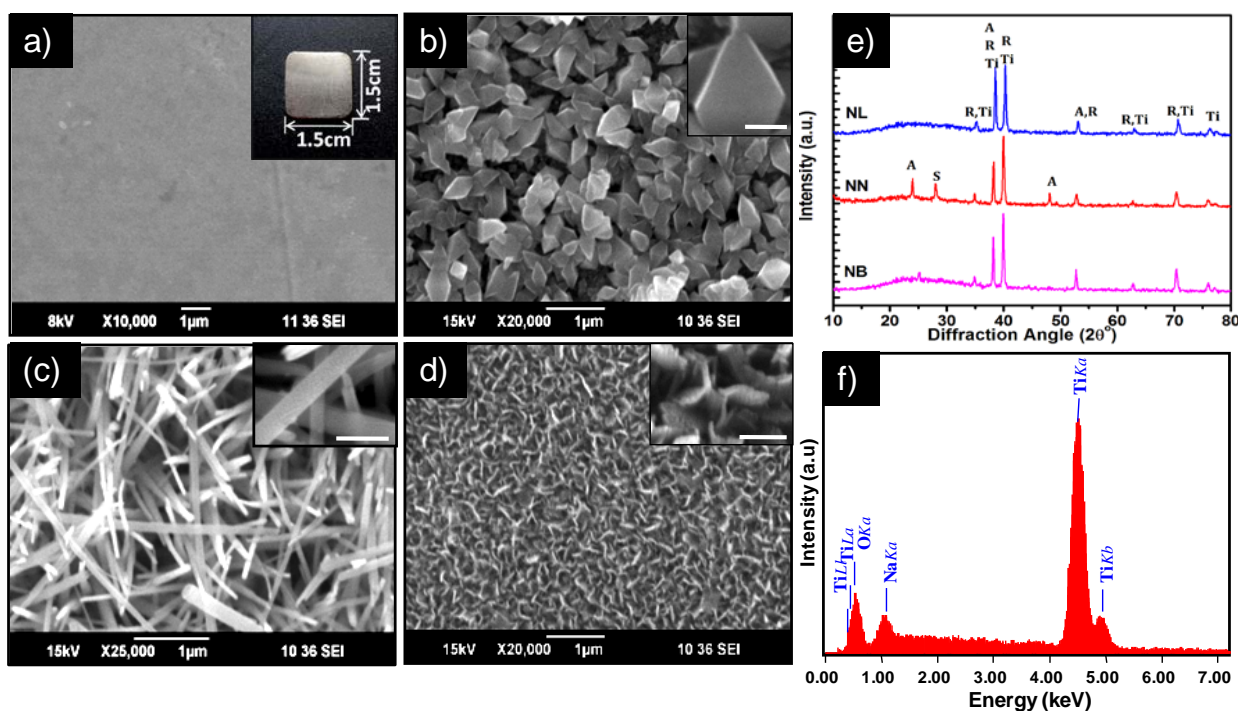


**Fig.1** SEM images of a) polished Ti plate (inset: photographic image of Ti plate), b) NB, c) NN, d) NL structures. (e) shows the XRD pattern of hydrothermally synthesized NL, NN and NB nanostructures (A- Anatase, R- Rutile, Ti- Titanium, S- sodium titanate). (f) corresponds to the EDS pattern of NL structures. Inset (b-d) shows the magnified view of NB, NN and NL structures (inset scale bar-200  $\mu\text{m}$ )

Cite this: DOI: 10.1039/c0xx00000x

www.rsc.org/xxxxxx

ARTICLE TYPE

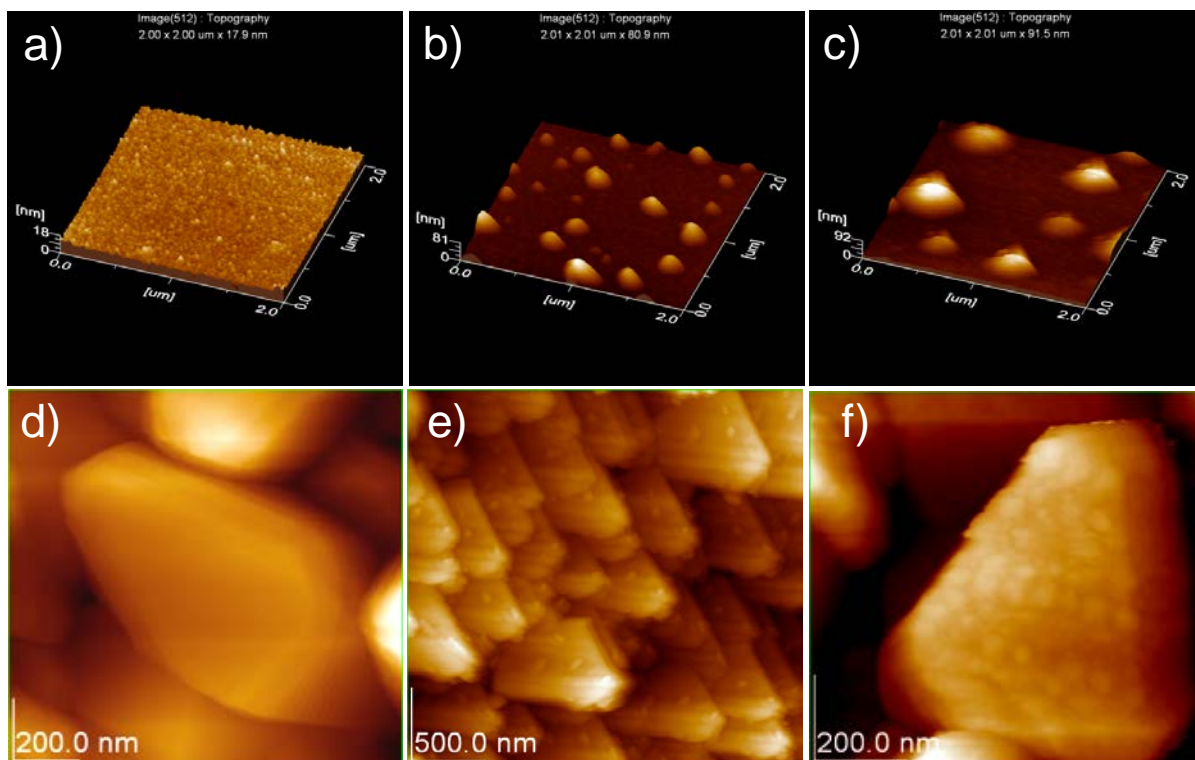


**Fig.2** AFM measurements: 3D view of topographic images of Ag sputtered mica sheets at different sputtering durations of (a) 25 s, (b) 75 s and (c) 100 s. Topographic image of NB structure before sputtering (scan size:  $1 \times 1 \mu\text{m}$ ) (d), after sputtering at 40 mA for 100 s imaged at scan size of  $2.5 \times 2.5 \mu\text{m}$  (e) and scan size of  $1 \times 1 \mu\text{m}$  (f).

5

Cite this: DOI: 10.1039/c0xx00000x

www.rsc.org/xxxxxx

## ARTICLE TYPE

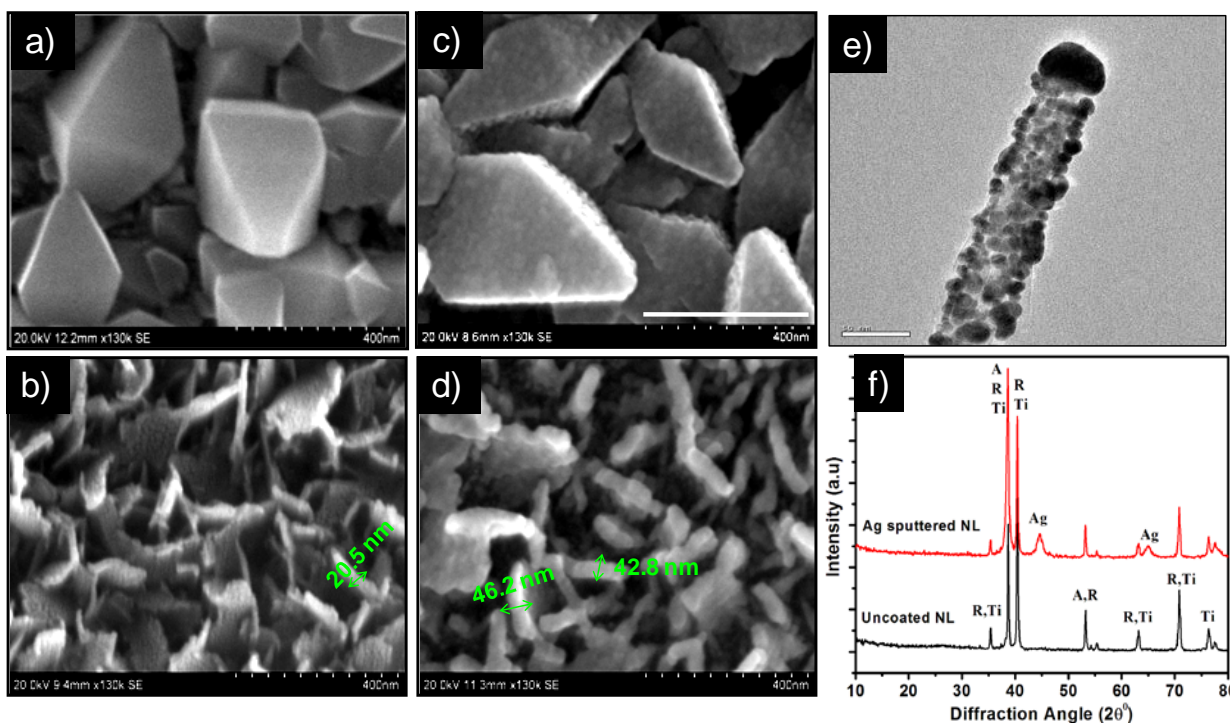


**Fig.3** FESEM images of NB (a,c) and NL (b,d) structures before Ag sputter deposition(a,b) and after Ag sputter deposition at 40 mA for 100 s (c,d), respectively, (e) TEM image of single needular structure deposited with Ag (scale bar: 50 nm). (f) shows the XRD pattern of Ag sputtered NL nanostructures (A- Anatase, R- Rutile, Ti- Titanium, Ag-silver).

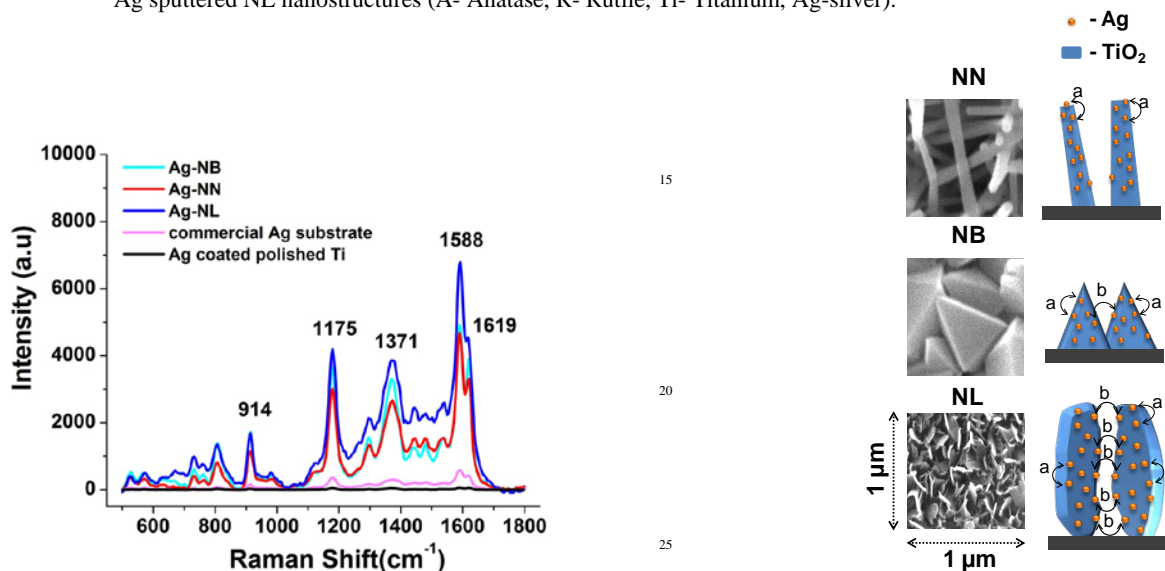


**Fig.4** Averaged SERS spectrum of 10 μM CV solution from NB, NN and NL substrates sputtered with Ag. The spectrum was also compared with commercial Ag SERS substrate and Ag coated polished Ti substrates (Integration time: 0.5 s, no of accumulations: 10)

**Fig.5** Formation of hot spots in Ag coated NN, NB and NL structures. (Left panel) SEM images of three nanostructures substrates showing a region within an area of 1 μm<sup>2</sup>. (Right panel) Schematic representing intra-structure (a) and inter-structure (b) hot spot formation within nanostructures.

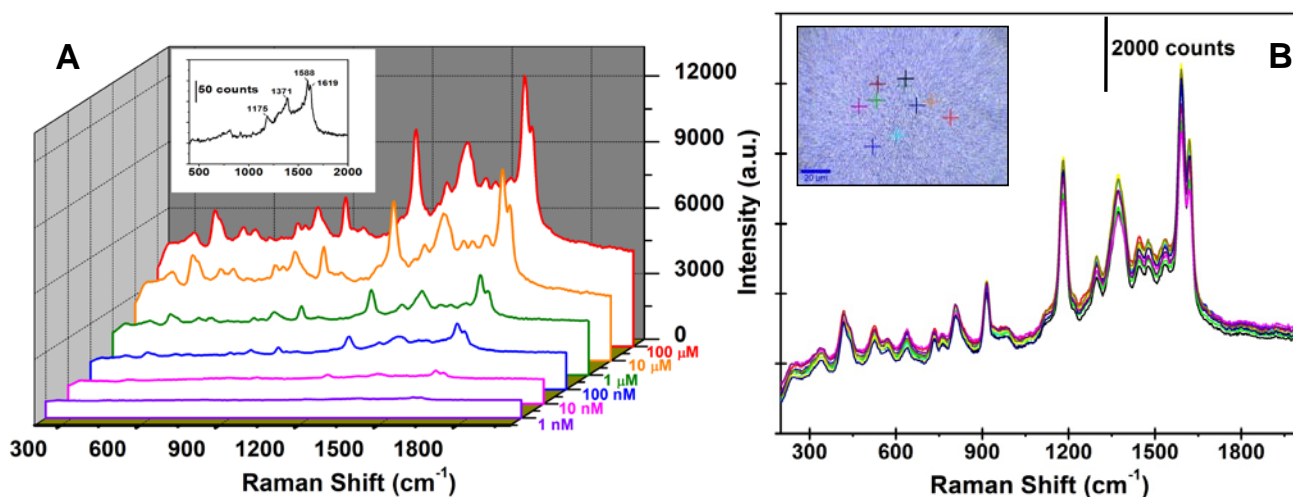


**Fig. 6** (A) SERS spectrum of CV recorded from Ag-NL substrates at different concentrations 1 nM, 10nm, 100nm, 1 $\mu$ M, 10  $\mu$ M, 100  $\mu$ M. Inset shows the spectra obtained at 1 nM showing the characteristic CV peaks at 1175, 1371, 1588 and 1619  $\text{cm}^{-1}$ . (B) SERS spectrum of CV (10  $\mu$ M) obtained from 10 random locations showing the reproducibility and uniformity of SERS signals from Ag-NL substrates. Inset shows the bright field image of NL substrate and the spots from which the spectrum was recorded (Integration time: 0.5 s, no of accumulations: 10).

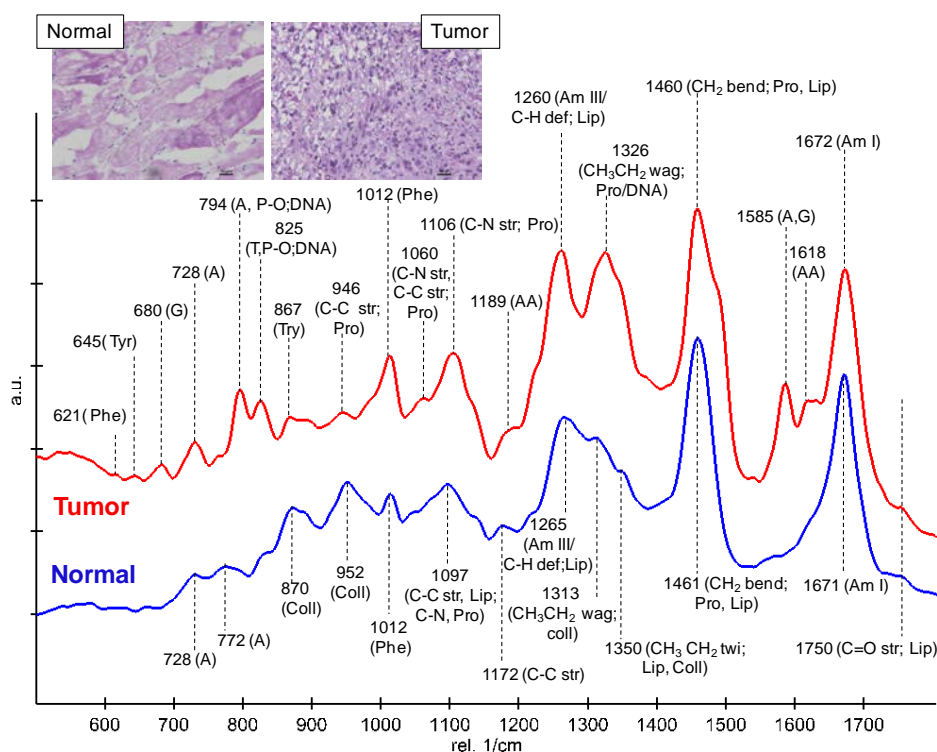


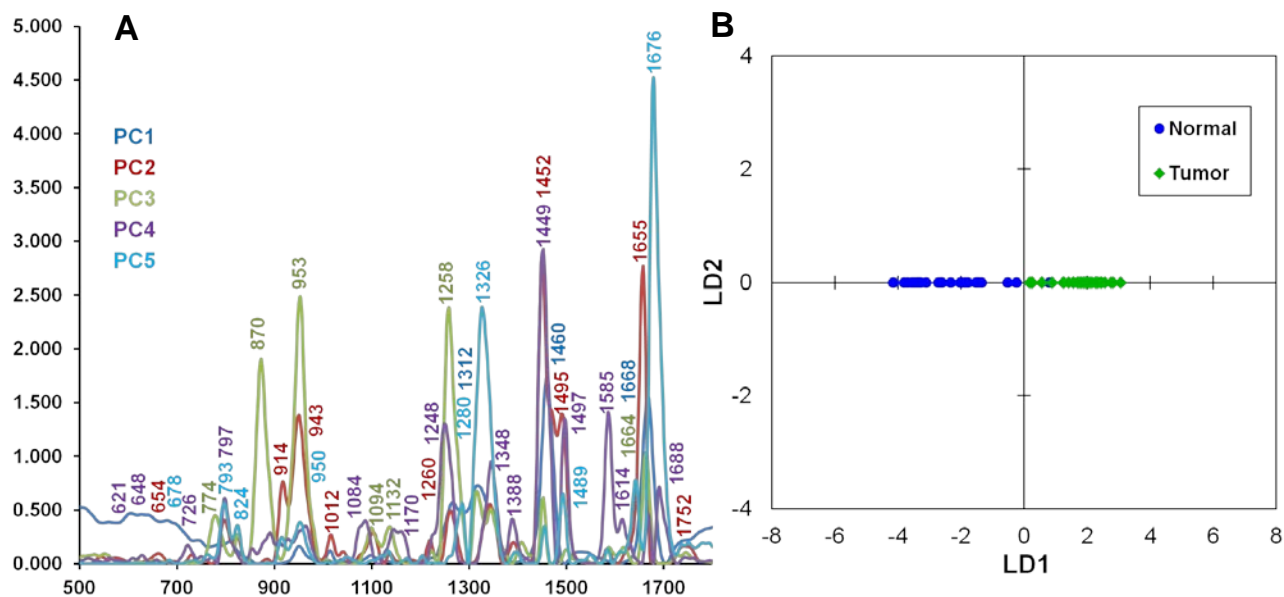
**Fig.7** Averaged SERS spectra of tumor and normal tissue obtained from Ag-NL substrates. Inset shows the H&E stained images of tumor and normal tissues. All the spectra were acquired with an integration time of 3 s. (A-adenine, G-guanine, T- thymine, Phe-phenyl alanine, Tyr- tyrosine, Try- tryptophan, P-O – phosphate, AA- aromatic amino acids, Pro- proteins, Lip- lipids, Coll- collagen, Am-amide; str- stretching, wag- wagging, bend- bending, twi- twisting vibrations)

15

Cite this: DOI: 10.1039/c0xx00000x

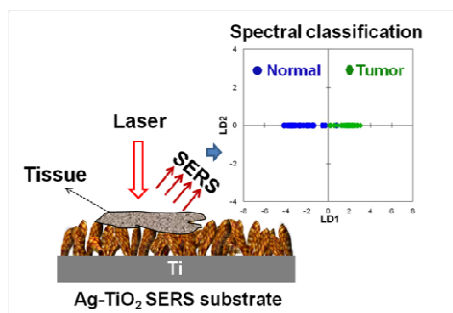
www.rsc.org/xxxxxx

ARTICLE TYPE



**Fig.8** Enhanced spectral features that contribute to the first five significant PCs (PC1 to PC5) of normal and tumor tissue spectra. Discriminant analysis bi-plot using linear discriminant scores (LD1, LD2) shows the classification of normal and tumor spectra. The specificity and sensitivity of classification estimated by cross-validation methods were 95.83% (23/24) and 100% (32/32), respectively.

5



Developed Ag-TiO<sub>2</sub> based large area surface-enhanced Raman spectroscopic (SERS) substrate that enables spectroscopic detection and classification of oral squamous cell carcinoma tissues with a specificity and sensitivity of 95.83% and 100%, respectively.